Article

Y-Shaped DNA Duplex Structure-Triggered Gold Nanoparticle Dimers for Ultrasensitive Colorimetric Detection of Nucleic Acid With The Dark-Field Microscope

Jingjing Li, Qingyun Liu, Hongyan Xi, Xiangcong Wei, and Zhengbo Chen

Anal. Chem., **Just Accepted Manuscript** • DOI: 10.1021/acs.analchem.7b03391 • Publication Date (Web): 09 Nov 2017

Y-Shaped DNA Duplex Structure-Triggered Gold Nanoparticle Dimers for Ultrasensitive Colorimetric Detection of Nucleic Acid With The Dark-Field Microscope

Jingjing Li,[1] Qingyun Liu,[2] Hongyan Xi,[1] Xiangcong Wei,[1] Zhengbo Chen[1]*

[1]Department of Chemistry, Capital Normal University, Beijing, 100048, China

[2]College of Chemistry and Environmental Engineering, Shandong University of Science and Technology, Qingdao, 266510, China

* Corresponding author. Tel.: 010-68903047

E-mail: czb979216@sina.com

ABSTRACT: Herein, we present a novel gold nanoparticle (AuNP) enumeration-based colorimetric aptamer biosensor for ultrasensitive detection of nucleic acid. This AuNP enumeration based colorimetric method takes advantages of the distinctive and strong localized surface plasmon resonance light scattering with the dark-field microscope. In our model system, first, cost-effective DNA1 instead of expensive 2-thioethyl ether acetic acid was capped on the surface of AuNPs to form dense DNA1 layer. Then, Two DNA strands (DNA2 and DNA3) in two different solutions were separately asymmetrically functionalized on the AuNPs capped the dense DNA1 layer. The subsequent binding of the target DNA could trigger the formation of perfect complementary DNA with Y shape, and adjust the distance between nanoparticles to form AuNP dimers, accompanied by a color change from green to yellow as observed, and thereby modulated the performance of the sensor, which resulted in the ultrahigh sensitivity. With this design, the 43 aM limit of detection was obtained, which exhibited an increase of at least 5-9 orders of magnitude in sensitivity over other colorimetric sensors fabricated using conventional strategies.

INTRODUCTION

Molecular bioassays act as an important diagnostic tool for the discrimination of disease-related biomarkers with significant research and clinical uses.[1] Typical target biomolecule such as nucleic acids is closely associated with some diseases, clinical diagnostics, drug screening, food safety, and environmental monitoring.[2-5] Thus, efficient and ultrasensitive detection of nucleic acids will offer an early disease diagnostic and help in the screening of andisease drugs. Currently, the most widely used methods to determine nucleic acids are optical and electrochemical measurements combined with the enzymatic or nonenzymatic amplification strategies.[6-14] These approaches have shown utility in early-stage disease detection.[15,16] However, nucleic acid detection depends primarily on target amplification strategies that require multiple time-consuming processing steps companied by some challenges related to successful primer design and library generation.[17,18] Moreover, fluorophore-based sensor for nucleic acid detection may suffer from hydrolysis,[19] self-quenching,[20] and dye bleaching[21] that result in low sensitivity and misidentification of potential biomarkers.[22]

Among these different sensing strategies, gold nanoparticles (AuNPs)-based colorimetric assays meet most of these requirements and have attracted enormous interest,[23-30] because of the accessibility of AuNP preparation, high molar extinction coefficient, easy surface modification, strong photostability, tunable optical properties, and so on.[31-33] Especially, the target-induced aggregation (or disaggregation) of AuNPs accompanied by the color change provides a simple signal readout for colorimetric detection of the target. Despite the impressive capabilities of AuNP aggregation or disaggregation-based colorimetric assays, there are three roadblocks that limit their practical applications especially in complex samples. First, AuNPs are extremely sensitive to the microenvironments including temperature, pH, salt concentration, and they are easy to form network-like aggregation. These aggregates are not stable in an aqueous solution due to the increase in the size of the particles and the decrease in the surface repulsive force.[34,35] Second, poor sensitivity. Most of the reported AuNP aggregation-based colorimetric methods reached a higher detection limit ($>$5 nM). The detection limit was several orders of magnitude higher than that of the assays based on fluorescence methods.[36] Third, narrow dynamic range. The linear

range of the sensors based on AuNP aggregation was only 1～2 orders of magnitude, which was much narrower than that of fluorescence methods.[37,38]

Inspired by the pioneering works of Guo et al.[39], Liu et al.[40,41], and Graham et al.[42], herein, we propose a novel, cost-effective, and ultrasensitive strategy for nucleic acid detection without involving any amplification step. The detection strategy is called the AuNP enumeration, which correlates the number of AuNPs with the amount of the target which is invisible under the dark-field microscope. The AuNP enumeration with the dark-field microscope represents a newly emerged methodology that offers an elegant route for sensitive biological assays. In the construction of the sensor, AuNPs were used as a colorimetric probe, where the nanoparticle surfaces were capped with the dense DNA1 layer and sparse DNA2 and DNA3. It is rather remarkable that cost-effective DNA1 instead of expensive 2-thioethyl ether acetic acid was utilized to maintain the stability of colloidal gold against complex conditions in real samples. DNA2 and DNA3 acted as the recognition units for detection of the target DNA. Since the amount of DNA1is far more than that of DNA2 and DNA3, and DNA1 sequence is shorter than DNA2 and DNA3, they run their functions independently without any interference. In the presence of the target DNA, DNA, DNA2, and DNA3 hybridized to form perfect complementary Y-shaped DNA duplexes. The generation of Y-shaped DNA duplexes could trigger the formation of AuNP dimers, accompanied by a color change from green to yellow as observed under dark-field microscope, leading to dramatic increase in yellow spots in dark-field images. Significantly, our detection system visualized the color signal because even extremely low concentration (43 aM) of the target DNA could induce the formation of AuNP dimers.

EXPERIMENTAL SECTION

Materials. Chloroauric acid ($HAuCl_4$) and trisodium citrate were purchased from Sigma-Aldrich. Tris-(2-carboxyethyl) phosphine hydrochloride (TCEP) was purchased from Alfa Aesar. DNA sequences were purchased by Sangon Biotechnology Inc. (Shanghai, China). The sequences of the oligonucleotides used in the experiments as follows: target DNA: 5'-CCT CGG TAG TAC CTA ATG ACA G-3', DNA1: 5'-SH-GGT GGT GGT GG-3', DNA2: 5'-SH-CTG TTA CTG TAC TAC CGA GG-3', DNA3: 5'-CTG TCA TTA GGC AGT AAC AG-SH-3', and random sequence: 5'- CCC CCC CCC CCC CCC-3'. All other reagents are of analytical reagent grade. Ultrapure water was provided by a Direct-Q3 system and used as a solvent in all experiments.

Instrumentation. The detection was performed using a microscope (DS-Fi2, Nikon). Transmission electron microscope (TEM) images were obtained on a Hitachi (H-7650, 80 kV) transmission electron microscope. Image-Pro Plus 6.0 software was used to process the dark-field microscopy images of AuNPs.

Synthesis of Gold Nanoparticles. AuNPs with 50 nm were prepared according to the previous literature.[43] Briefly, 200 μL of 1% sodium citrate was added quickly into 30 mL of 0.01% $HAuCl_4 \cdot 3H_2O$ solution under vigorous stirring in an oil-bath at 100 °C. The solution turned red rapidly, indicating the formation of 50 nm AuNPs (10 nM). The resulting solution was cooled to room temperature under mild stirring and stored at 4 °C prior to use.

Preparation of DNA Modified AuNPs. Prior to the preparation of DNA-AuNP conjugates, DNA1, DNA2, and DNA3 were processed as follows: each DNA (1 μM) including 1 mM TCEP (TCEP was employed to reduce the possible disulfide bonds in DNA sequences to thiols) in Tris-HCl buffer (20 mM, pH 7.40 with 140 mM NaCl, and 20 mM $MgCl_2$) was heated to 85°C for 5 min, and then cooled to room temperature. Then, 15 μL of 0.1 μM the treated DNA1 was added to 450 μL of 25 pM AuNP solution for 24 h at 37°C. Next, 7.5 μl of 0.1 μM DNA2-functionalized AuNP solution and 7.5 μl of 0.1μM DNA3-functionalized AuNP solution were mixed with the above DNA1-capped AuNP solution for 24 h at 37°C, and the DNA2 and DNA3 were anchored on the remaining active sites of DNA1-capped AuNPs.

Detection of the Target DNA. The detection of target DNA was performed as follows: the target DNA with various concentrations was mixed with 53 μL of Tris-HCl buffer and 450 μL of DNA1-capped AuNPs functionalized with DNA2 and DNA3. The mixed solution was incubated for 2 h at 37 °C for binding of the target DNA. Finally, we sucked 30 μL of the above solution, and slightly dripped on the glass slide. The glass slide was immediately covered with a coverslip. The sensor was ready for observation under the dark-field microscopy.

RESULTS AND DISCUSSION

Sensing Mechanism. The rationale of the proposed colorimetric assay combines the non-specific DNA1 functionalized AuNPs and the perfect complementary Y-shaped DNA strategy. As illustrated in **Scheme 1**, the non-specific DNA1was first modified on the surfaces of AuNPs to form dense DNA1 layer. Then, two probes (DNA2 and DNA3) were immobilezed onto the DNA1-functionalize AuNPs in two separate solutions, respectively. Each DNA sequence of DNA2 and DNA3) includes two parts: one part and a portion of the other DNA sequence are complementary, and the other is complementary to a portion of the sequence of the target DNA (**Scheme 1**B). In the absence of the target DNA, the mixture of DNA2-functionalized AuNPs and DNA3-functionalized AuNPs could not form DNA duplexes owing to lower melting temperature than the operating temperature, preventing the formation of Y-shaped DNA duplex structure. Whereas the presence of the target DNA induced the formation of Y-shaped DNA duplexes, because in this case, the T_m was above the operation temperature, thereby drawing the AuNPs closer to form AuNP dimers, indicative of some yellow dots under dark-field microscopy observation.

Scheme 1. (A) Schematic Illustration of Nucleic Acid Detection Based on AuNP Enumeration with A Dark-Field Microscope. (B) The Formation of A Complementary Y-Shaped DNA Duplex.

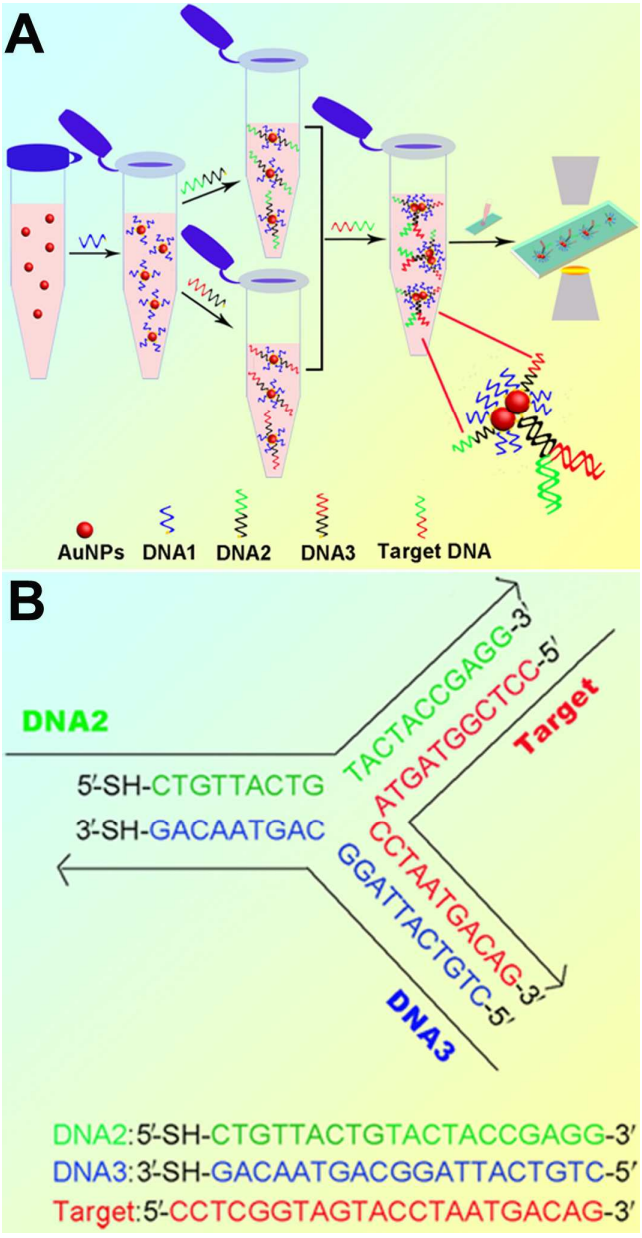

Condition Optimization. In order to achieve better analytical performance, several experimental parameters such as AuNP concentration, DNA1 concentration, and DNA1/DNA2 or DNA1/DNA3 concentration ratio, were optimized. As shown in **Fig. 1**(A_1-D_1, E), the number of yellow AuNPs increased with the AuNP concentration up to 25 pM and exhibited no further increase compared with the blank with extra addition of the AuNPs in the presence of 0.1 pM targe DNA. Thus, 25 pM AuNPs was employed for the following use. The amount of DNA1 is an important factor that exerts influence on the analytical performance of the sensor. It is basically required that the amount of DNA1 functionalized AuNPs is high enough to avoid the formation of large AuNP aggregates. To obtain AuNP dimers, DNA1 with varied concentrations (0, 1, 3, 5, 7 and 10 nM) was used to functionalize AuNPs (25 pM) to adjust the density of DNA1 on the surface of AuNPs. As shown in **Fig. 2**, the AuNP counts increased sharply with the increasing concentration of DNA1 from 0 to 7 nM and decreased quickly beyond 7 nM. Moreover, after adding the DNA1, we introduced potassium ions again to trigger the DNA1 to form G-quadruplex structure. Surprisingly, no obvious variations of dark-field color were observed, due to the fact that no AuNP dimers were formed. We presume that G-quadruplex structure may afford a big steric effect on its neighboring DNA2 and DNA3, and thus prevent the formation of Y-shaped DNA duplex structure between DNA2 and DNA3 modified on the surface of AuNPs. In contrast, in the absence of potassium ions, 7 nM DNA1-modified AuNPs eliminated the steric hindrance effect, which allowed the formation of structurally reproducible AuNP dimers. The influence of the concentration ratio of DNA1/DNA2 (the concentration ratio of DNA2/DNA3=1) was investigated by monitoring the dark-field image signal. As shown in **Fig. 3**, the AuNP counts increased slowly with an increase of the DNA1/DNA2 concentration ratio up to 4:1, and further increased sharply from 4:1 to 2:1. Therefore, the optimal concentration ratio of DNA1/DNA2 was 4:1.

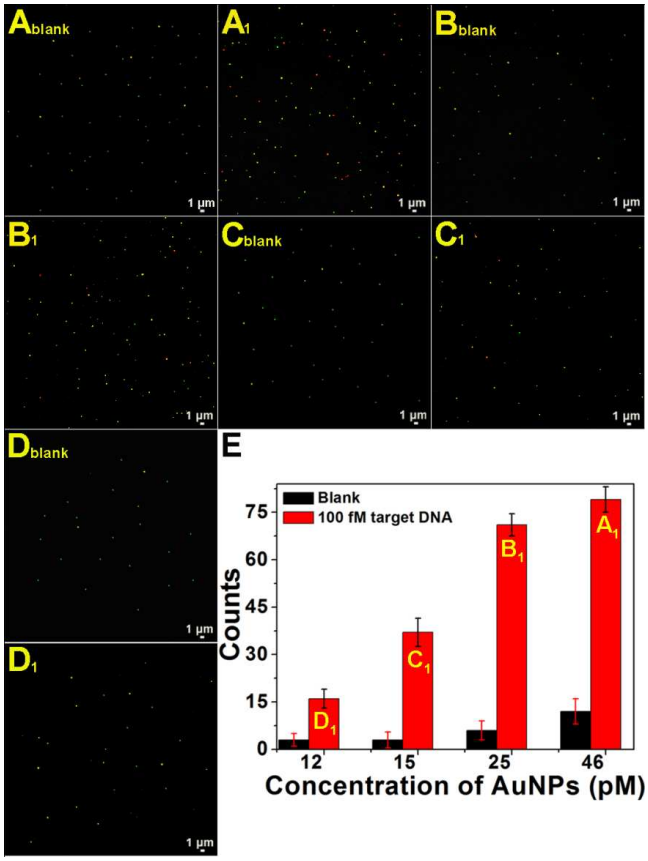

Figure 1. Dark-field images of different concentrations of AuNPs (D_1: 12, C_1: 15, B_1: 25, and A_1: 46 pM) in the absence (A_{blank}-D_{blank}) and presence (A-D) of 0.1 pM target DNA. (E) AuNP counts as a function of AuNP concentration in the absence and presence of the target DNA. Error bars represent the standard deviation of triplicates.

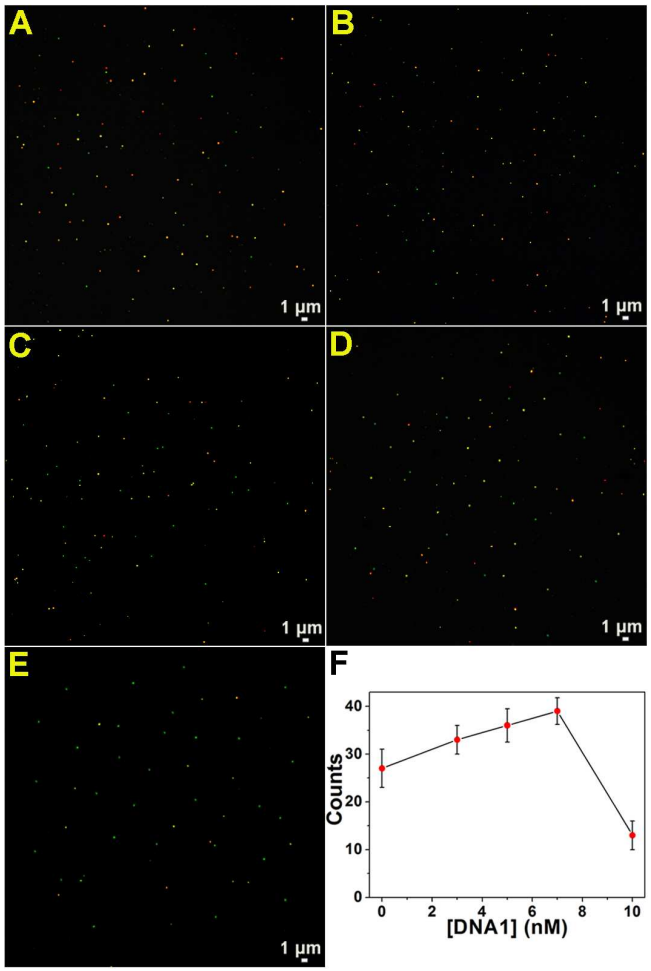

Figure 2. Dark-field images of AuNPs in the presence of DNA1 with various concentrations. (A) 0, (B) 3, (C) 5, (D) 7, and (E) 10 nM. (F) Effect of different DNA1 concentrations on the AuNP counts. Error bars represent the standard deviation of triplicates.

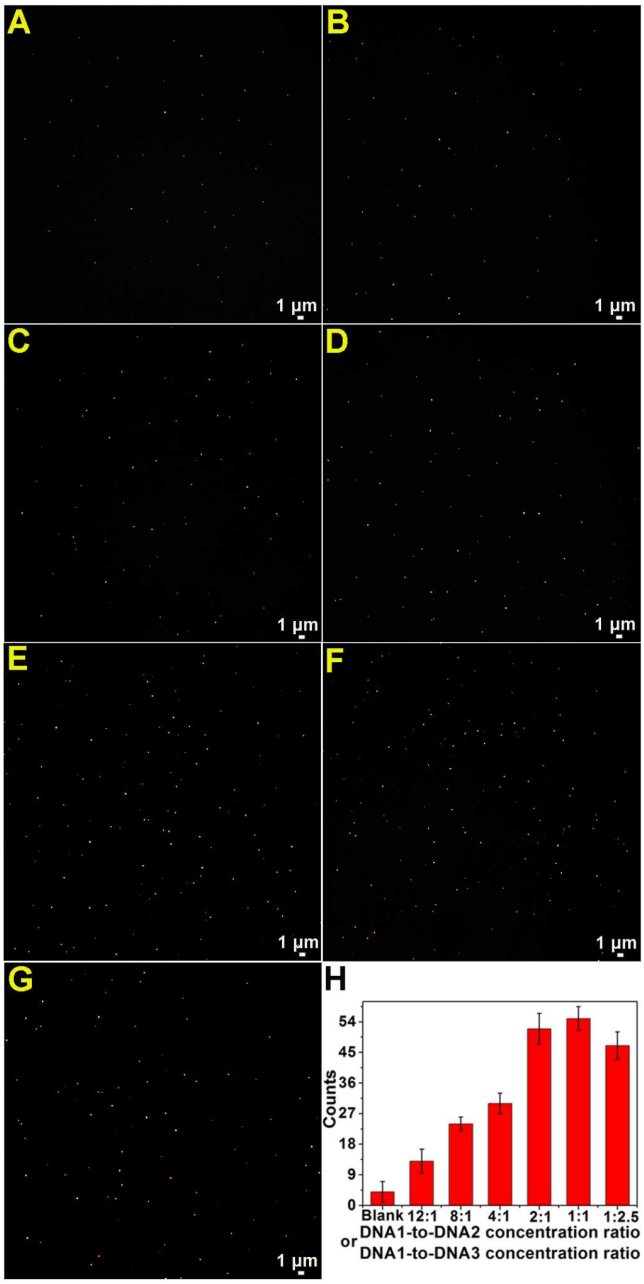

Figure 3. Dark-field images of AuNPs in the presence of different concentration ratios of DNA1/DNA2: (A) blank, (B) 12:1, (C) 8:1, (D) 4:1, (E) 2:1, (F) 1:1, and (G) 1:2.5. (H) AuNP counts in response to DNA1/DNA2 concentration ratios. Error bars represent the standard deviation of triplicates.

Sensing Performance. Under the optimal experimental conditions, the target DNA with different concentrations was added to the reaction system to evaluate the analytical performance of the colorimetric platform. Since the concentration of the target DNA is closely related to the number of yellow AuNPs, the amount of the target DNA can thus be determined by counting the number of yellow AuNPs in the dark-field image. As shown in **Fig. 4**(D-I), the number of yellow AuNPs increased with increasing the target DNA concentration. This finding indicated that, with the increase of the target DNA concentration, more complementary Y-shaped duplexes were formed, thus inducing the formation of Y-shaped DNA linked

AuNP dimers, resulting in an increase in number of yellow AuNP dimers. **Fig. 4**A shows the AuNP counts as a function of the target DNA concentration. The target DNA with concentrations expanding from 0.1 to 1000 fM was able to be quantified (**Fig. 4**C) with the limit of detection (LOD) at 43 aM (by the 3σ/k rule, n=3) (**Fig. 4**B). This enormous improvement in sensitivity could be ascribed the reason as follows: for a nonoriented colorimetric sensor, the interparticle distance was not small enough to generate detectable colorimetric responses when small aggregates were formed. Thus, when an excess of the target DNA existed, a colorimetric change could only be observed. However, for our designed oriented sensor, even with extremely low concentration of the target DNA could form the Y-shaped DNA duplex structure, which can induce AuNP dimer formation. Therefore, a target DNA with extremely low concentration could be detected. TEM images further demonstrated the formation of AuNP dimers (**Fig. 5**). As presented, the DNA1, DNA2, and DNA3-functionalized AuNPs were well dispersed in the solution. However, the existence of the target DNA caused the formation of the Y-shaped DNA linked AuNP dimers, indicative of a lot of yellow AuNPs in dark-filed images (**Fig. 4**(G-I)).

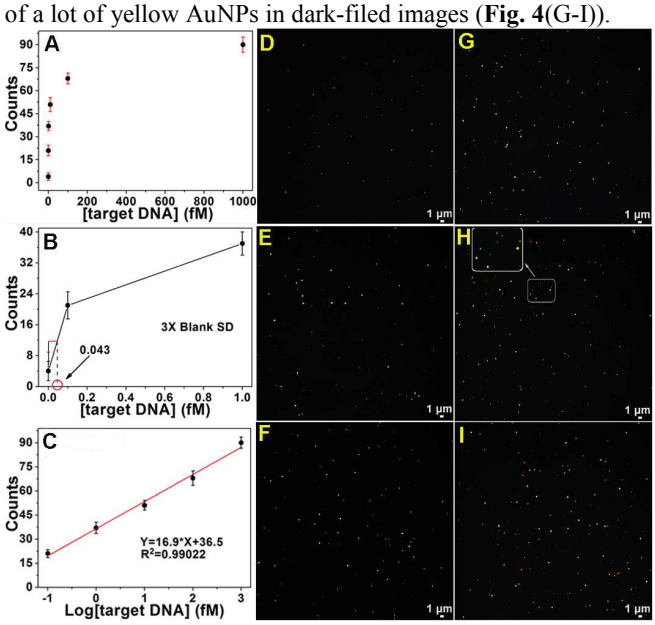

Figure 4. (A) The AuNP counts as a function of the target DNA concentration. (B) Calculation of the detection limit of the target DNA in the presence of Y-shaped DNA-linked AuNP dimers. (C) The linear relationship between the AuNP counts and the logarithm of the target concentration ranging from 0.1 to 1000 fM. Dark-field images of AuNPs with different concentrations of the target DNA: (D) 0, (E) 0.1fM, (F) 1fM, (G) 10 fM, (H) 0.1 pM, and (I)1 pM. The illustrated error bars represent the standard deviation of triplicates.

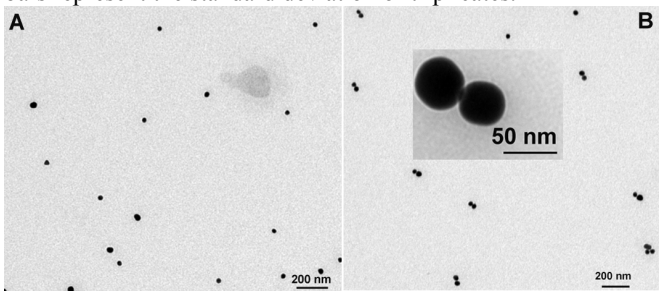

Figure 5. Representative TEM images of (A) DNA-functionalized AuNPs, and (B) the Y-shaped DNA linked AuNP dimers in the presence of 10 fM target DNA.

The Selectivity. The oriented sensor was also challenged with a random sequence of 15-nucleotide DNA to examine its selectivity. Color changes observed from the dark field images and AuNP counts as a function of the concentration of a random sequence and the target DNA were shown in **Fig. 6**. Remarkably, the color changes in the dark field images could not be observed (**Fig. 6**(G-L)), and AuNP counts had negligible responses to the concentration of the random sequence (**Fig. 6**M), suggesting that the random sequence did not exert interference on the sensor. Whereas only the presence of the target DNA could induce the AuNP dimers (**Fig. 6**(A-F, M)), which affirmed that the AuNP dimers could be mainly attributed to the formation of complementary Y-shaped DNA duplexes. Of note, in the presence of 1 pM random sequence, a linear relationship between AuNP counts and logarithm of the target DNA in the range from 0.1 fM to 1pM was still obtained (**Fig. 6**N) with the LOD of 0.05 fM (**Fig. 6**O). This result indicated that interference from the random sequence was negligible and the nonspecific absorption was not significant in the detection.

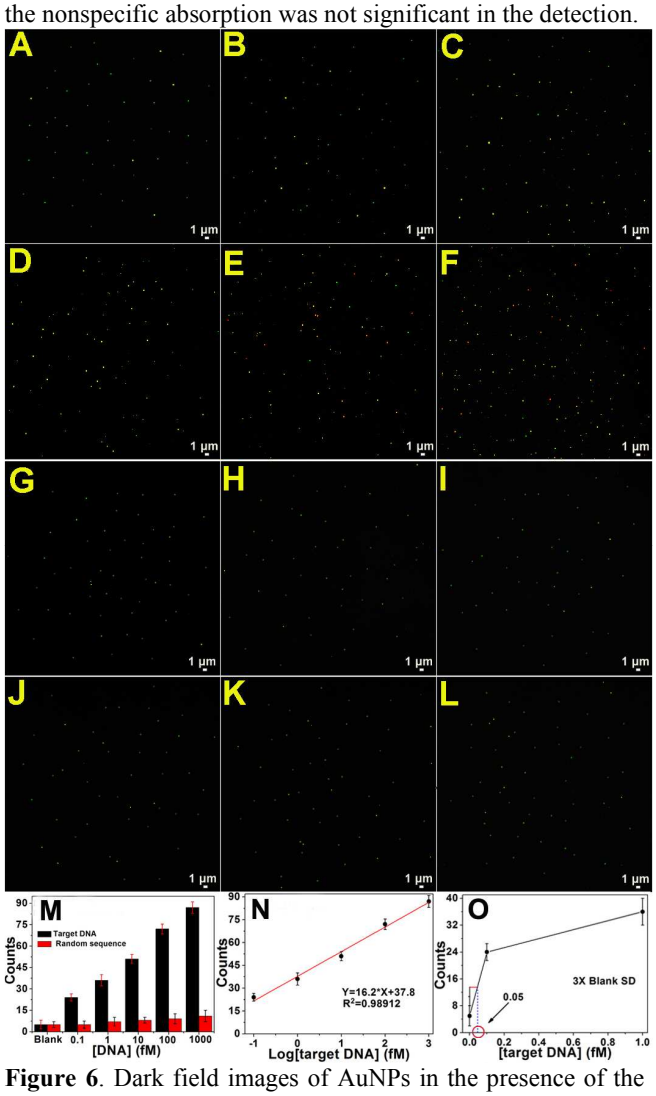

Figure 6. Dark field images of AuNPs in the presence of the target DNA(A-F) and random sequence (G-L). The target DNA concentration: (A) 0, (B) 0.1fM, (C)1fM, (D)10 fM, (E)

0.1 pM, and (F)1pM. The random sequence concentration: (G) 0, (H) 0.1fM, (I)1fM, (J)10 fM, (K) 0.1pM, and (L)1pM. (M) AuNP counts as a function of the concentration of the target DNA and a random sequence. (N) The logarithm plot of AuNP counts versus target DNA concentrations (0.1 fM-1 pM). (O) Calculation of the detection limit of the target DNA in the presence of a random sequence. The illustrated error bars represent the standard deviation of triplicates.

The Feasibility. In order to test the applicability of the oriented sensor for the rapid and ultrasensitive DNA assay, real human serum samples collected from Chinese PLA General Hospital (Beijjing, China) were tested. Various concentrations of target DNA were respectively spiked in these serum samples and these spiked samples were subsequently tested by using the proposed oriented sensor. As depicted in **Fig. 7**, the performance of the colorimetric sensor in the target DNA detection in serum was almost the same as that in Tris buffer. In these solutions, the AuNP counts was linear with the logarithm of the target DNA concentrations expanding from 0.1 fM to 1 pM, and the detection limit of the target DNA was calculated to be 51 aM. The results revealed that (a) the Y-shaped DNA linked AuNP dimers were highly stable in the complex serum samples, (b) the unknown substance in the serum had almost no influence on the analytical performance of the sensor, and (c) the Y-shaped DNA duplex-linked AuNP enumeration with the dark-field microscope enabled a variety of merits for detection of oligonucleotides especially in complex environment. However, oligonucleotide detection in these complex samples was difficult to be realized with conventional methods.

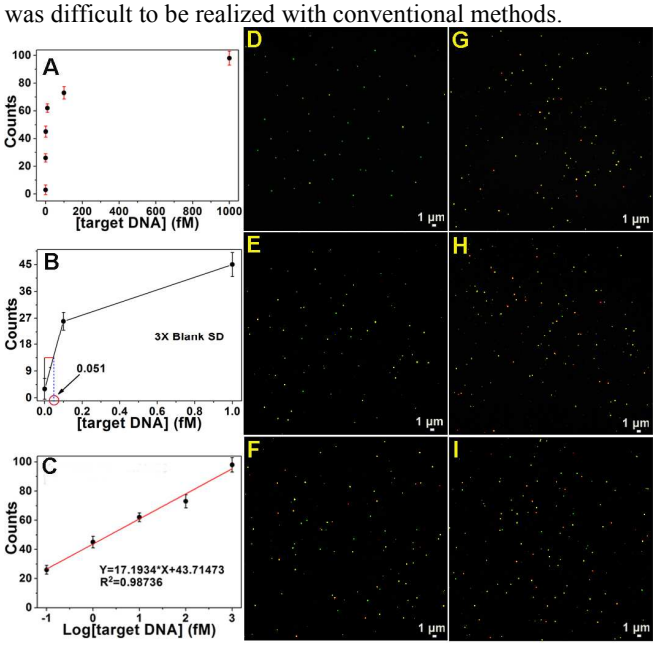

Figure 7. (A) The AuNP counts as a function of the target DNA concentration. (B) Calculation of the detection limit of the target DNA in human serum sample. (C) The linear relationship between the AuNP counts and the logarithm of the target DNA ranging from 0.1 fM to 1 pM. Dark-field images of Y-shaped DNA linked AuNPs with different concentrations of the target DNA: (D) 0, (E) 0.1 aM, (F) 1 fM, (G) 10 fM, (H) 0.1 pM, and (I) 1 pM. Error bars represent the standard deviation of triplicates.

CONCLUSIONS

In summary, we have successfully demonstrated a target oligonucleotide-programmed AuNP dimerization strategy for ultrasensitive detection of nucleic acid based on AuNP enumeration signal readout mode with the dark-field microscope. The proposed sensing platform possessed several special advantages over conventional AuNP aggregation-based colorimetric systems in the sensitivity (aM vs nM), the signal output (AuNP counts vs intensity variations), and the cost of materials (oligonucleotide vs 2-thioethyl ether acetic acid). This massive improvement in detection sensitivity could be mainly attributable to the rational design of two DNA sequences for hybridizing with target DNA in Y-shaped manner, which could render the Au NPs much closer to form AuNP dimers. The core of the colorimetric assay was to build AuNP count signal readout mode to evaluate whether AuNPs aggregated, reflected by the color change from green to yellow under dark-field microscopy observation. The AuNP counting as a means of signal readout avoided the attachment of the expensive spectrometer to the dark-field microscope setup and the effect of the heterogeneity of size and morphology of nanoparticles on the detection sensitivity. Additionally, oligonucleotide with -SH modification wss far cheaper than 2-thioethyl ether acetic acid, in consideration of cost saving, the study of nucleic acid sensors made from thiol-oligonucleotide instead of 2-thioethyl ether acetic acid is advisable. Finally, it is worth mentioning that the selection criteria of dimers can be much improved by combining a hyper-spectral imaging system in front of a conventional imaging CCD camera.[44]

AUTHOR INFORMATION

Corresponding Author

* Phone: +86-010-68903047. E-mail: czb979216@sina.com

Notes

The authors declare no competing financial interest.

ACKNOWLEDGMENT

This study was supported by Scientific Research Project of Beijing Educational Committee (Grant No. KM201710028009), Youth Innovative Research Team of Capital Normal University, and the Project of Construction of Scientific Research Base by the Beijing Municipal Education Commission.

REFERENCES

(1) D. A., Giljohann, C. A. Mirkin, *Nature* **2009**, *462*, 461-464.

(2) R. Frank, R. Hargreaves, *Nat. Rev. Drug Discovery* **2003**, *2*, 566-580.

(3) H. Q. Zhang, F. Li, B. Dever, X. F. Li, X. C. Le, *Chem. Rev*. **2013**, *113*, 2812-2841.

(4) W. Zhou, X. Gao, D. B. Liu, X. Y. Chen, *Chem. Rev.* **2015**, *115*, 10575-10636.

(5) H. Liang, X. B. Zhang, Y. F. Lv, L. Gong, R. W. Wang, X. Y. Zhu, R. H. Yang, W. H. Tan, *Acc. Chem. Res.* **2014**, *47*, 1891-1901.

(6) T. G. Drummond, M. G. Hill, J. K. Barton, *Nat. Biotechnol*. **2003**, 21, 1192-1199.

(7) J. S. Sun, Y. L. Xianyu, X. Y. Jiang, *Chem. Soc. Rev.* **2014**, *43*, 6239-6253.

(8) B. A. Du, Z. P. Li, C. H. Liu, *Angew. Chem., Int. Ed*. **2006**, *45*, 8022-8025.

(9) X. Y. Xu, D. G. Georganopoulou, H. D. Hill, C. A. Mirkin, *Anal. Chem*. **2007**, *79*, 6650-6654.

(10) L. D. Wang, R. J. Deng, J. H. Li, *Chem. Sci*. **2015**, *6*, 6777-6782.

(11) Z. Wu, G. Q. Liu, X. L. Yang, J. H. Jiang, *J. Am. Chem. Soc.* **2015**, *137*, 6829-6836.

(12) Y. L. Hu, H. X. Jia, Y. C. Wang, Y. Q. Cheng, Z. P. Li, *Chem. Commun*. **2014**, *50*, 13093-13095.

(13) X. J. Liao, Q. B. Wang, H. X. Ju, *Chem. Commun*. **2014**, *50*, 13604-13607.

(14) P. He, W. P. Qiao, L. J. Liu, S. S. Zhang, *Chem. Commun.* **2014**, *50*, 10718-10721.

(15) X. Chen, Y. Ba, L. J. Ma, X. Cai, Y. Yin, K. H. Wang, J. G. Guo, Y. J. Zhang, J. N. Chen, X. Guo, *Cell Res*. **2008**, *18*, 997-1006.

(16) I. Visintin, Z. Feng, G. Longton, D. C. Ward, A. B. Alvero, Y. L. Lai, J. Tenthorey, A. Leiser, R. Flores-Saaib, H. Yu, C*lin. Cancer Res.* **2008**, *14*, 1065-1072.

(17) M. Baker, *Nat. Methods* **2010**, *7*, 687-692.

(18) S. Goodwin, J. D. McPherson, W. R. McCombie, *Nat. Rev. Genet*. **2016**, *17*, 333-351.

(19) P. J. Hrdlicka, B. R. Babu, M. D. Sorensen, N. Harrit, J. Wengel, *J. Am. Chem. Soc*. **2005**, *127*, 13293-13299.

(20) P. Wilkins Stevens, J. G. Hall, V. Lyamichev, B. P. Neri, M. Lu, L. Wang, L. M. Smith, D. M. Kelso, *Nucleic Acids Res*. **2001**, *29*, E77.

(21) B. N. Giepmans, S. R. Adams, M. H. Ellisman, R. Y. Tsien, *Science* **2006**, *312*, 217-224.

(22) A. H. Alhasan, D. Y. Kim, W. L. Daniel, E. Watson, J. J. Meeks, C. S. Thaxton, C. A. Mirkin, *Anal. Chem*. **2012**, *84*, 4153-4160.

(23) D. A. Giljohann, D. S. Seferos, W. L. Daniel, M. D. Massich, P. C. Patel, C. A. Mirkin, *Angew. Chem., Int. Ed*. **2010**, *49*, 3280-3294.

(24) D. Kato, M. Oishi, *ACS Nano* **2014**, *8*, 9988-9997.

(25) W. Shen, H. M. Deng, Z. Q. Gao, *J. Am. Chem. Soc*. **2012**, *134*,14678-14681.

(26) R. de la Rica, M. M. Stevens, *Nat. Nanotechnol.* **2012**, *7*, 821-824.

(27) R. Elghanian, J. J. Storhoff, R. C. Mucic, R. L. Letsinger, C. A. Mirkin, *Science* **1997**, *277*, 1078-1081.

(28) N. L. Rosi, C. A. Mirkin, *Chem. Rev.* **2005**, *105*, 1547-1562.

(29) K. Saha, S. S. Agasti, C. Kim, X. N. Li, V. M. Rotello, *Chem. Rev.* **2012**, *112*, 2739-2779.

(30) L. A. Lane, X. Qian, S. Nie, *Chem. Rev.* **2015**, *115*, 10489-10529.

(31) J. J. Du, L. Jiang, Q. Shao, X. G. Liu, R. S. Marks, J. Ma, X. D. Chen, *Small* **2013**, *9*, 1467-1481.

(32) W. Chansuvarn, T. Tuntulani, A. Imyim,*TrAC, Trends Anal. Chem.* **2015**, *65*, 83-96.

(33) E. Oliveira, C. Nunez, H. M. Santos, J. Fernandez-Lodeiro, A. Fernandez-Lodeiro, J. L. Capelo, C. Lodeiro, *Sens. Actuators, B* **2015**, *212*, 297-328.

(34) J. J. Storhoff, A. A. Lazarides, R. C. Mucic, C. A. Mirkin, R. L. Letsinger, G. C. Schatz, *J. Am. Chem. Soc*. **2000**, *122*, 4640-4650.

(35) N. T. K. Thanh, Z. Rosenzweig, *Anal. Chem*. **2002**, *74*, 1624-1628.

(36) M. S. T. Gonçalves, *Chem. Rev*. **2009**, *109*, 190-212.

(37) S. R. Opperwall, A. Divakaran, E. G. Porter, J. A. Christians, A. J. DenHartigh, D. E. Benson, *ACS Nano* **2012**, *6*, 8078-8086.

(38) A. Vallee-Belisle, F. Ricci, K. W. Plaxco, *J. Am. Chem. Soc*. **2012**, *134*, 2876-2879.

(39) L. H. Guo, Y. Xu, A. R. Ferhan, G. N. Chen, D. H. Kim, *J. Am. Chem. Soc.* **2013**, *135*, 12338-12345.

(40) W. Zhou, Q. Li, H. Q. Liu, J. Yang, D. B. Liu, *ACS Nano* **2017**, *11*, 3532-3541.

(41) Y. M. Xiong, M. M. Li, H. Q. Liu, Z. H. Xuan, J. Jiang, D. B. Liu, *Nanoscale* **2017**, *9*, 1811-1815.

(42) D. Graham, D. G. Thompson, W. E. Smith, K. Faulds, *Nature Nanotech.* **2008**, *3*, 548-551.

(43) N. G. Bastus, J. Comenge, V. Puntes, *Langmuir* **2011**, *27*, 11098-11105.

(44) M. Iga, N. Kakuryu, T. Tanaami, J. Sajiki, K. Isozaki, T. Itoh, *Rev. Sci. Instrum*. **2012**, *83*, 103707.

for TOC only

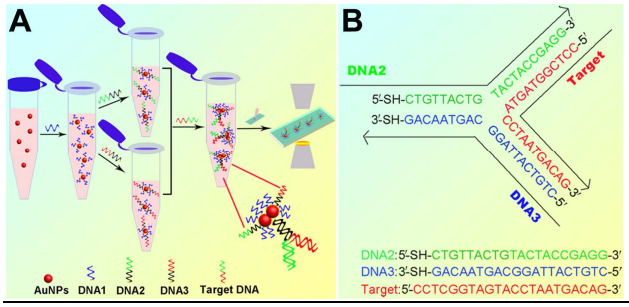
A
AuNPs
DNA1
DNA2
DNA3
Target DNA
B
DNA2
5'-SH-CTGTTACTG
3'-SH-GACAATGAC
TACTACCGAGG-3'
ATGATGGCTCC-5'
Target
CCTAATGACAG-3'
GGATTACTGTC-5'
DNA3
DNA2:5'-SH-CTGTTACTGTACTACCGAGG-3'
DNA3:3'-SH-GACAATGACGGATTACTGTC-5'
Target:5'-CCTCGGTAGTACCTAATGACAG-3'